

Observation of query pulse length dependent Ramsey interference in rubidium vapor using pulsed Raman excitation

G. S. Pati,^{1,*} F. K. Fatemi,² and M.S. Shahriar³

¹Department of Physics and Pre-Engineering, Delaware State University, Dover, Delaware 19901, USA

²Optical Sciences Division, Naval Research laboratory, Washington, DC 20375, USA

³Department of Electrical Engineering and Computer Science, Northwestern University, Evanston, Illinois 60308, USA

*gspati@desu.edu

Abstract: We report observation of query pulse length dependent Ramsey interference (QPLD-RI), using pulsed Raman excitation in rubidium vapor. This is observed when a long, attenuated query pulse is used during pulsed Raman excitation. We explain the physical mechanism behind the QPLD-RI using a Bloch vector model. We also use numerical solutions to time-dependent density matrix equations to simulate this interference effect, showing qualitative agreement with experimental results. Presence of such interference could create a potential source of error in a vapor cell Raman clock constructed using frequency-domain Ramsey interference (FDRI).

©2011 Optical Society of America

OCIS codes: (270.1670) Coherent optical effects; (300.6320) Spectroscopy, high-resolution.

References and links

1. N. F. Ramsey, "A molecular beam resonance method with separated oscillating field," *Phys. Rev.* **78**(6), 695–699 (1950).
2. M. M. Salour and C. Cohen-Tannoudji, "Observation of Ramsey's interference fringes in the profile of Doppler-free two-photon resonances," *Phys. Rev. Lett.* **38**(14), 757–760 (1977).
3. G. Theobald, V. Giordano, N. Dimatcq, and P. Cerez, "Observation of narrow Ramsey-type resonances in a caesium beam due to Zeeman coherences," *J. Phys. B* **24**(13), 2957–2966 (1991).
4. B. Schuh, S. I. Kanorsky, A. Weis, and T. W. Hänsch, "Observation of Ramsey fringes in nonlinear Faraday rotation," *Opt. Commun.* **100**(5-6), 451–455 (1993).
5. A. S. Zibrov and A. S. Matsko, "Optical Ramsey fringes induced by Zeeman coherence," *Phys. Rev. A* **65**(1), 013814 (2001).
6. A. S. Zibrov, I. Novikova, and A. B. Matsko, "Observation of Ramsey fringes in an atomic cell with buffer gas," *Opt. Lett.* **26**(17), 1311–1313 (2001).
7. L. Essen and J. V. L. Parry, "An atomic standard of frequency and time interval: a caesium resonator," *Nature* **176**(4476), 280–282 (1955).
8. A. G. Mungall, H. Daams, and J. S. Boulanger, "Design, construction, and performance of the NRC CsVI primary cesium clocks," *Metrolog.* **17**(4), 123–145 (1981).
9. C. Audoin, "Caesium beam frequency standards: classical and optically pumped," *Metrolog.* **29**(2), 113–134 (1992).
10. J. Thomas, P. R. Hemmer, S. Ezekiel, C. C. Leiby, R. H. Picard, and C. R. Willis, "Observation of Ramsey fringes using a stimulated resonance Raman transition in a sodium atomic beam," *Phys. Rev. Lett.* **48**(13), 867–870 (1982).
11. P. R. Hemmer, S. Ezekiel, and C. C. Leiby, Jr., "Stabilization of a microwave oscillator using a resonance Raman transition in a sodium beam," *Opt. Lett.* **8**(8), 440–442 (1983).
12. P. R. Hemmer, M. S. Shahriar, H. Lamela-Rivera, S. P. Smith, B. E. Bernacki, and S. Ezekiel, "Semiconductor laser excitation of Ramsey fringes using a Raman transition in a cesium atomic beam," *J. Opt. Soc. Am. B* **10**(8), 1326–1329 (1993).
13. T. Zanon, S. Guerandel, E. de Clercq, D. Holleville, N. Dimarcq, and A. Clairon, "High contrast Ramsey fringes with coherent-population-trapping pulses in a double lambda atomic system," *Phys. Rev. Lett.* **94**(19), 193002 (2005).
14. G. S. Pati, K. Salit, R. Tripathi, and M. S. Shahriar, "Demonstration of Raman–Ramsey fringes using time delayed optical pulses in rubidium vapor," *Opt. Commun.* **281**(18), 4676–4680 (2008).

15. G. S. Pati, F. K. Fatemi, M. Bashkansky, and S. Shahriar, "Prospect for development of a pulsed CPT Raman-Ramsey clock using atomic vapor," *Proc. SPIE* **7612**, 76120D, 76120D-25 (2010).
16. B. Yan, Y. Ma, and Y. Wang, "Formation of Ramsey fringes based on pulsed coherent light storage," *Phys. Rev. A* **79**(6), 063820 (2009).
17. M. Merimaa, T. Lindvall, I. Tittonen, and E. Ikonen, "All-optical atomic clock based on coherent population trapping in Rb," *J. Opt. Soc. Am. B* **20**(2), 273–279 (2003).
18. J. Vanier, "Atomic clocks based on coherent population trapping: a review," *Appl. Phys. B* **81**(4), 421–442 (2005).
19. G. S. Pati, F. K. Fatemi, M. Bashkansky, and S. Shahriar, "Optical Ramsey interference and its performance in D1 line excitation in rubidium vapor for implementation of a vapor cell clock," *Proc. SPIE* **7949**, 794910D (2010).
20. V. Shah, S. Kanppe, P. D. Schwindt, and J. Kitching, "Subpicotesla atomic magnetometry with a microfabricated vapour cell," *Nat. Photonics* **1**(11), 649–652 (2007).
21. E. Arimondo, "Coherent population trapping in laser spectroscopy," in *Progress in Optics*, E. Wolf, ed. (Elsevier, 1996), Vol. 35, pp. 257–354.
22. M. S. Shahriar, P. R. Hemmer, D. P. Katz, A. Lee, and M. G. Prentiss, "Dark-state-based three-element vector model for the stimulated Raman interaction," *Phys. Rev. A* **55**(3), 2272–2282 (1997).
23. P. R. Hemmer, M. S. Shahriar, V. D. Natoli, and S. Ezekiel, "AC Stark shifts in a two-zone Raman interaction," *J. Opt. Soc. Am. B* **6**(8), 1519–1528 (1989).
24. P. R. Hemmer, G. P. Ontai, and S. Ezekiel, "Precision studies of stimulated-resonance Raman interactions in an atomic beam," *J. Opt. Soc. Am. B* **3**(2), 219–230 (1986).
25. S. Brandt, A. Nagel, R. Wynands, and D. Meschede, "Buffer-gas-induced line width reduction of coherent dark resonances to below 50 Hz," *Phys. Rev. A* **56**(2), R1063–R1066 (1997).
26. S. J. Park, H. Cho, T. Y. Kwon, and H. S. Lee, "Transient coherence oscillation induced by a detuned Raman field in a rubidium Λ system," *Phys. Rev. A* **69**(2), 023806 (2004).

1. Introduction

Optical (or microwave) fields separated in space (or time) can interfere to produce Ramsey fringes via the coherence induced by the atomic polarization [1]. During such a process, the coherence is transported by an atom (or molecule) and interference is produced by the read-out field depending on the phase difference between the oscillating field and the coherence. Over the years, several papers have reported Ramsey interference using different schemes such as the Doppler-free two-photon resonance, ground-state Zeeman coherence and polarization rotation, and suggested their applications in precision metrology [2–6]. Some of these studies have also shown interference resulting from atomic diffusion where a coherently prepared atom escapes and reenters the interaction region with a residual phase memory [5,6].

Frequency-domain Ramsey fringes are generated by changing the frequency of the oscillatory field away from the atomic resonance during interrogation. This method was originally applied to separated field microwave interactions in an atomic beam to yield narrower atomic resonances [7]. It is now widely used in the development of cesium beam atomic clocks [8,9]. Later, separated-field Raman interaction using a three-level Λ -system was developed to replace the microwave interaction in the atomic beam by an all-optical interaction while generating Ramsey interference [10–12]. The interference produced by this scheme is commonly referred to as Raman Ramsey interference (RRI).

Recently, an extension of this approach to time-domain has been studied in atomic vapor cells with renewed interest [13–16]. This technique can be applied to realize a potentially high-performance vapor cell Raman clock compared to that using coherent population trapping (CPT) [17,18]. In a recent study, we have shown that high-contrast frequency-domain Ramsey interference (FDRI) fringes with sub-kilohertz linewidth can be produced in coherently prepared ^{85}Rb atomic vapor [19]. A repeated sequence of time-separated optical Raman pulses was used to generate FDRI fringes.

In this paper, we show a new type of Ramsey interference effect using a similar pulsed excitation mechanism in rubidium vapor. Unlike FDRI, these fringes are observed as time-domain oscillations in the transmission amplitude of a long, attenuated query pulse. As discussed later, the frequency of these oscillations is inversely related to the Raman detuning, and the number of observed oscillations depends on the duration (or length) of the query pulse. We refer to them as query pulse length dependent Ramsey interference (QPLD-RI).

We use a Bloch vector model to provide a clear physical explanation of RRI observed in the form of FDRI and QPLD-RI. We also use a numerical model to describe the dynamics of the Λ -system under pulsed Raman excitation, agreeing closely with our experimental results. Keeping in mind a possible high-performance vapor cell clock development, we have also explored the magnetic field dependence of FDRI and QPLD-RI using a clock transition in ^{85}Rb atom. RRI can also be used in sensitive magnetometry [20] if Zeeman sublevels with first order magnetic field sensitivity are used in Raman transitions during pulsed Raman excitation.

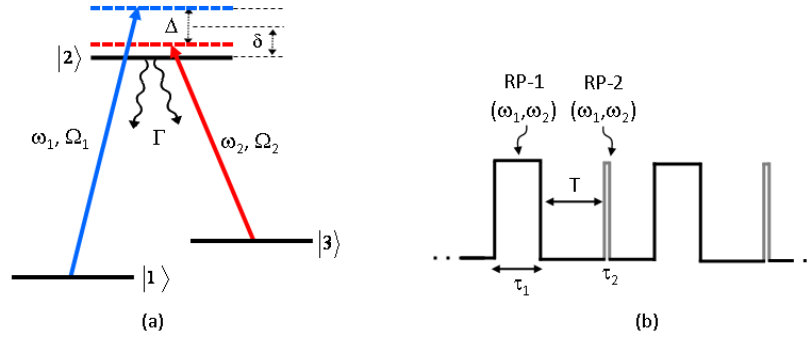


Fig. 1. (a) Raman excitation in a three-level Λ -system: ω_1 and ω_2 correspond the frequencies of the Raman beams, Δ and δ correspond to the difference (or two-photon) and average frequency detuning, respectively (b) repeated sequence of Raman pulse (RP) used in generating Ramsey interference.

Our study shows that QPLD-RI can produce pulse length dependent broadening as well as asymmetry in FDRI fringes used for a vapor cell Raman clock, causing a potential source of error. Specifically, we show that broadening affects the fractional frequency stability of a clock, and asymmetry changes the magnitude of the light-shift induced error due to optical detuning, which is unavoidable in a vapor cell based Raman clock because of the presence several hyperfine transitions in the excited state manifold, which all contribute to the clock signal because of Doppler broadening. Thus, in choosing the optimal parameters for such a clock, the effect of QPLD-RI has to be taken into account.

2. Theoretical description

Two-photon resonant Raman excitation in a three-level Λ -system forms the basis for both QPLD-RI and FDRI to be discussed here. Figure 1a shows such a scheme. Here, ω_1 and ω_2 are the frequencies of the two excitation fields, detuned from resonance by δ_1 and δ_2 , respectively; Ω_1 and Ω_2 correspond to the Rabi frequencies for the two legs; $\delta \equiv (\delta_1 + \delta_2)/2$ is the average detuning of the two fields, and $\Delta \equiv (\delta_1 - \delta_2)$ is the difference detuning, which is also called the two-photon detuning or the Raman detuning. We assume that the excited state population decays equally to the two metastable ground states, with a net decay rate of Γ . If the Raman beams are continuous, CPT resonance can be observed in the transmitted laser field [21–24]. On the other hand, if the atomic medium is excited by a repeated sequence of pulsed Raman beams as shown in Fig. 1b, RRI can be observed. In this case, a relatively long pulse (duration τ_1) is used first to prepare the atoms in the CPT state, also known as the dark state $(|-\rangle) = (\Omega_2 |1\rangle - \Omega_1 |2\rangle) / \sqrt{\Omega_1^2 + \Omega_2^2}$. After a free evolution time, T , another Raman pulse of short duration τ_2 is used as a detection pulse to observe Ramsey interference. The interference is created by the second pulse via the atomic coherence induced by the first Raman/CPT pulse. Short detection (or query) pulse is generally used in order to avoid any significant perturbation of coherence produced by the first pulse [14]. Choosing a longer τ_2

will tend to suppress the interference effect unless one uses a strongly attenuated query pulse, as discussed in greater detail later. Experimentally, the interference fringes are observed by measuring the transmitted amplitude of the short detection pulse using electronic gating and time integration while changing the interference condition by changing the difference frequency, Δ , between the Raman beams. To gain further insight into the origin of Raman Ramsey interference phenomena and their characteristics, here we will use a three-element Bloch vector (BV) model [22] to describe the time evolution of the Λ -system under pulsed Raman excitation and explain the formation of FDRI and QPLD-RI.

If we consider the decay rate Γ of the excited state to be much greater than any other rates in the Λ -system, the unpopulated atomic state $|2\rangle$ can be eliminated from the interaction picture using an adiabatic approximation. Such an approximation is fairly consistent with our experimental study of interest. In this case, the time evolution of the Λ -system can be represented by the motion of a three-element BV. The components of BV can be described by the density matrix elements of the atomic states $|1\rangle$ and $|3\rangle$ alone. The BV in this case, is somewhat analogous to the BV of a two-level system, and has been discussed at length for Raman excitation in ref. 22.

A partially diagonalized basis consisting of the dressed states $|\mp\rangle = \frac{1}{\sqrt{2}}(|1\rangle \mp |3\rangle)$ for $\Omega_1 = \Omega_2 = \Omega$ provides the simplest interpretation for the BV model. The equation of motion for the Raman BV vector [22] is given by

$$\dot{\vec{R}} = \vec{Q} \times \vec{R} - \alpha \vec{R} + \alpha \hat{e}_3 \quad (1)$$

where $\vec{R} = R_1 \hat{e}_1 + R_2 \hat{e}_2 + R_3 \hat{e}_3$ is the BV, and $\vec{Q} = -\Delta \hat{e}_1 + \beta \hat{e}_3$ is the so-called torque vector. The three real elements (R_1, R_2, R_3) of the BV are defined in terms of the density matrix elements in the dressed basis as $\rho_{-+} = \frac{1}{2}(R_1 + iR_2)$, and $\rho_{--} - \rho_{++} = R_3$. The parameter $\alpha = \Omega_R^2/2\Gamma = \Omega^2/2\Gamma$ corresponds to the Raman pumping rate, $\beta = \Omega_R^2 \delta / (\Gamma^2 + 4\delta^2)$ corresponds to the frequency difference between $|+\rangle$ and $|-\rangle$ states which in our discussion is generally considered to be negligibly small (i.e. $\beta \approx 0$), and $\Omega_R = \sqrt{\Omega_1^2 + \Omega_2^2}$ is the Raman Rabi frequency. Thus, the motion of the BV is primarily governed by the choice of parameters α and Δ . For a closed atomic system, $\rho_{--} + \rho_{++} = 1$. Note that the Raman BV does not conserve its amplitude at all times due to the presence of decay of \vec{R} and growth of R_3 (second and third terms in Eq. (1)). As can be seen from Eq. (1), it can start from zero amplitude, and grow into a maximum steady-state amplitude of one. This is to be contrasted with the case of a two level system without decay (e.g., a microwave transition under ideal conditions). In such a system, the length of the BV is conserved. However, if decay is included in a two level system (e.g., an optical transition where the upper level decays rapidly), the length of the BV is also not conserved, even if the system is closed.

Note that the BV described above can also be expressed in the atomic basis as $\vec{R} = \tilde{R}_1 \hat{e}_1 + \tilde{R}_2 \hat{e}_2 + \tilde{R}_3 \hat{e}_3$, where $\rho_{13} = \frac{1}{2}(\tilde{R}_1 + i\tilde{R}_2)$ and $\rho_{11} - \rho_{33} = \tilde{R}_3$. The \hat{e}_i basis is related to the \hat{e}_i basis by a rotation of angle 2θ in the 1-3 plane, where $\tan \theta = \Omega_1 / \Omega_2$ [22]. For the case of $\Omega_1 = \Omega_2$, the angle of rotation is $2\theta = \pi/2$, so that $R_1 = \tilde{R}_3, R_2 = \tilde{R}_2, R_3 = -\tilde{R}_1$. This corresponds to the following explicit relations between the elements of the density matrix in these two bases: $\text{Re}(\rho_{13}) = -(\rho_{--} - \rho_{++})/2$, $\text{Im}(\rho_{13}) = \text{Im}(\rho_{-+})$, and $\rho_{11} - \rho_{33} = 2\text{Re}(\rho_{-+})$.

However, the dynamics of the system is more transparent in the dressed states basis [22]; hence, we use this basis throughout this paper.

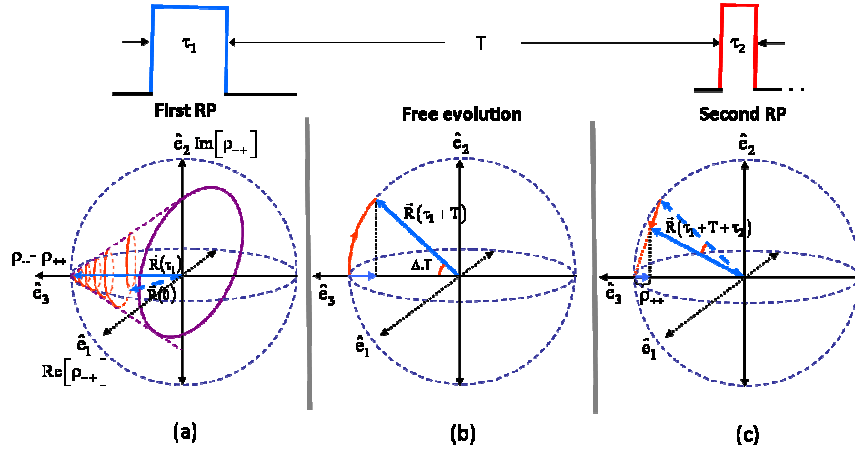


Fig. 2. Bloch vector model showing the dynamics of a three-level Λ -system during pulsed Raman excitation. The figures show the BVs (a) after interaction with the first Raman/CPT pulse (dotted blue arrow: start of BV; solid blue arrow: end state of BV) (b) during free evolution time, T , and (c) after interaction with the second Raman (or detection) pulse.

The rotation of the Raman BV during interaction with the pulsed Raman beams, and during free-time evolution, T , can be described as follows. The first CPT pulse (shown in Fig. 1b) causes a strong interaction due to higher pulse intensity and long τ_1 . Under this condition, we can assume that $\alpha \gg |\Delta|$ and $\alpha \tau_1 \gg 1$. This causes the system to reach the steady state after interaction with the first pulse. The steady state solution to the equation of motion in Eq. (1) is found from $\ddot{\vec{R}} = 0$, which indicates formation of a complete dark state described by the BV $\vec{R}(\tau_1) = 1 \cdot \hat{e}_3$ with $R_3 = 1$. This also corresponds to $\rho_{--} = 1$, $\rho_{++} = 0$, $\rho_{-+} = 0$. Figure 2a shows pictorially evolution of the BV starting from $\vec{R}(0)$, indicated by the dotted blue arrow, to $\vec{R}(\tau_1)$, indicated by the solid blue arrow, during interaction with the first pulse, for $|\beta| \gg |\Delta|$. Under this condition, the torque vector is $\vec{Q} \approx \beta \hat{e}_3$, which causes the spiraling motion around the \hat{e}_3 axis. For the case of $\beta = 0$, the BV simply moves to the steady state value in a straight line, starting from any initial value [22]. To illustrate the motion of the BV in the free evolution zone and the query pulse zone, we assume $\beta = 0$ in these zones.

In the absence of interaction during the free evolution time T , $\alpha = 0$. Under this condition, one can no longer ignore the two-photon detuning, Δ , which causes the Bloch vector \vec{R} to precess at a rate Δ around the \hat{e}_1 -axis, as shown in Fig. 2b. Using Eq. (1), one can find the Raman BV at time $t = \tau_1 + T$ as $\vec{R}(\tau_1 + T) = \sin(\Delta T) \hat{e}_2 + \cos(\Delta T) \hat{e}_3$. This implies that at the end of time T , the BV sweeps a total angle $\theta (= \Delta T)$. For example, if $\Delta = 0$, the BV does not rotate and $\vec{R}(\tau_1 + T) = 1 \cdot \hat{e}_3$. During interaction of the atoms with a repeated sequence of Raman pulses, Δ can be changed slowly around $\Delta = 0$, thus, causing the BV $\vec{R}(\tau_1 + T)$ to oscillate in the $(\hat{e}_2 - \hat{e}_3)$ plane. The effect of this oscillation can be observed by measuring the absorption of a second Raman (or detection) pulse which is present during the time $t = \tau_1 + T$ and $t = \tau_1 + T + \tau_2$.

The BV at $t = \tau_1 + T$ serves as the initial BV for interaction with the second Raman pulse. It is assumed that the optical fields in the second Raman pulse have the same phase as that of the first Raman pulse so that the motion of the BV simply continues from where it was left off at the end of time $t = \tau_1 + T$. During this interaction in the query zone, we also assume $\alpha \gg |\Delta|$ in Eq. (1), and the motion of the BV is described as $\vec{R}(\tau_1 + T + \tau_2) = \sin(\Delta T) e^{-\alpha \tau_2} \hat{e}_2 + [1 - (1 - \cos(\Delta T) e^{-\alpha \tau_2})] \hat{e}_3$. While observing FDRI, τ_2 is kept short so that $\alpha \tau_2 \approx 0$, and the Raman BV practically remains unchanged after interaction with the second pulse. This effect is shown in Fig. 2c. It is obvious that if τ_2 is made long, the BV will eventually grow linearly to the steady state BV given by $\vec{R}_y = 1 \cdot \hat{e}_3$, indicating the formation of a new dark state. The transmitted amplitude of the second pulse directly corresponds to the projected BV component R_3 ($\approx \cos(\Delta T)$), which is also a measure of the dressed state population difference ($\rho_{--} - \rho_{++}$). FDRI is observed as oscillations in R_3 caused due to change in Δ during repeated interaction with the pulse sequence. The frequency width of these fringes is inversely related to T , and is not affected by power broadening.

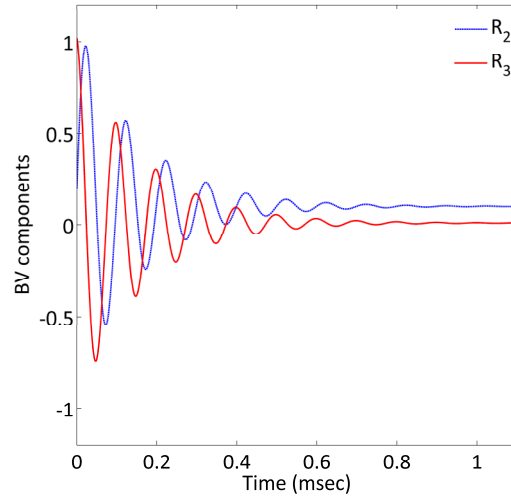


Fig. 3. Plots showing oscillations in BV components R_2 and R_3 as a function of τ_2 for $\Delta = 10$ KHz, $\alpha = 0.1 \Delta$ and $T = 100 \mu\text{s}$.

The BV model also explains the new type of Ramsey interference, QPLD-RI. This interference is observed when the amplitude of the second Raman pulse is significantly attenuated and the duration τ_2 of the pulse is made long. In this case, the motion of the BV in the query zone is governed by both α and Δ . Using appropriate initial conditions at $t = \tau_1 + T$, the solution to Eq. (1) is obtained as

$$\vec{R}(\tau_2) = \left[\left[\sin(\Delta(\tau_2 + T)) - \cos \theta \cdot \sin(\Delta(\tau_2 + \theta)) \right] e^{-\alpha \tau_2} + \frac{\sin 2\theta}{2} \right] \hat{e}_2 + \left[\left[\cos(\Delta(\tau_2 + T)) - \cos \theta \cdot \cos(\Delta(\tau_2 + \theta)) \right] e^{-\alpha \tau_2} + \frac{1 + \cos 2\theta}{2} \right] \hat{e}_3 \quad (2)$$

where $\theta = \arccos\left(\frac{\alpha}{\sqrt{\alpha^2 + \Delta^2}}\right)$. The projected BV component R_3 describes the Ramsey interference observed in the transmitted amplitude of the query pulse as a function of τ_2 . It contains two damped oscillatory terms decaying at a rate of α . Figure 3 shows the oscillations in BV components R_2 and R_3 as a function of τ_2 . We chose $\Delta = 10$ KHz, and $\alpha = 0.1 \Delta$ for this case. Also, since $\alpha \ll |\Delta|$, $\theta \approx 90^\circ$, in this case, the BV can be approximated as $\vec{R}(\tau_2) \approx \sin(\Delta(\tau_2 + T)) e^{-\alpha\tau_2} \hat{e}_2 + \cos(\Delta(\tau_2 + T)) e^{-\alpha\tau_2} \hat{e}_3$. One can draw the following conclusions about QPLD-RI. Temporal width of these fringes is inversely related to Δ . The fringes will disappear if Δ is matched to the two-photon resonance condition (i.e. $\Delta = 0$). The initial phase of the oscillation is determined by T . Decay time of the fringes is inversely related to the Raman pumping rate α of the query pulse. The present BV model does not include ground-state decoherence, γ and its effect on the decay of QPLD-RI.

Even though this model provides a simple understanding of the dynamics of the Ramsey interference, a quantitative modeling using time-dependent density matrix equations is necessary for describing these interference phenomena more accurately. We will briefly describe the basic density matrix equations and present our numerical simulation results using such a model. The density matrix equations for a three-level atomic system are described by the Liouville equation:

$$\dot{\tilde{\rho}} = -\frac{i}{\hbar} [\tilde{H}, \tilde{\rho}] + \dot{\tilde{\rho}}_{decay} \quad (3)$$

where $\tilde{\rho}$ represents the density operator in the rotating-wave basis consisting of nine matrix elements for a three-level system. $\dot{\tilde{\rho}}_{decay}$ describes various possible relaxation terms between the atomic levels. The diagonal elements of $\tilde{\rho}$ correspond to the population terms satisfying the condition $\tilde{\rho}_{11} + \tilde{\rho}_{22} + \tilde{\rho}_{33} = 1$ for a closed system, and the off-diagonal elements correspond to the coherence between various atomic levels created due to interaction with the laser fields. The interaction Hamiltonian for such a three-level system in the time independent basis is given by

$$\tilde{H} = \begin{pmatrix} 0 & \frac{\Omega_1}{2} & 0 \\ \frac{\Omega_1}{2} & -\delta & \frac{\Omega_2}{2} \\ 0 & \frac{\Omega_2}{2} & -\Delta \end{pmatrix} \quad (4)$$

where the parameters are as defined earlier in Fig. 1. Interaction of the atoms with the Raman pulse sequence and generation of Ramsey interference can be described by an exact solution to eight independent time-dependent equations given in Eq. (3). We obtained the numerical solutions to these equations during three sequential time intervals τ_1 , T , and τ_2 respectively, and used the solution from one time interval as the initial values for the next time interval.

Figure 4a shows a typical example of numerically computed FDRI fringes. For this case, we used a Raman pulse sequence with parameters $\tau_1 = 4 \times 10^3 \cdot (1/\Gamma)$ [$\approx 212 \mu\text{s}$ for $\Gamma = 2\pi(6 \text{ MHz})$], $T = 795 \mu\text{s}$, and $\tau_2 = 1 \mu\text{s}$. The Rabi frequencies for the Raman beams were taken to be equal, and weak compared to the excited state decay rate: $\Omega_1 = \Omega_2 = 2\pi(\Gamma/10)$, and δ was set equal to zero. Amplitude of FDRI, in this case, was calculated by finding the integrated

signal $\int_{\tau_1+T}^{\tau_1+T+\tau_2} \text{Im}[\rho_{13}] \cdot dt$ as a function Δ . The linewidth, $\Delta\nu$ of the Ramsey fringe, centered around $\Delta = 0$, agrees closely with $1/2T$ (≈ 628.9 Hz). For a rectangular shape of the Raman/CPT pulse, the frequency spread of the FDRI envelope is described by $\text{sinc}^2(\Delta\tau_i/2)$, which corresponds to the Fourier transform of the CPT pulse. Here, we have used the function *sinc*, which is defined as $\text{sinc}(x) \equiv \sin(x)/x$.

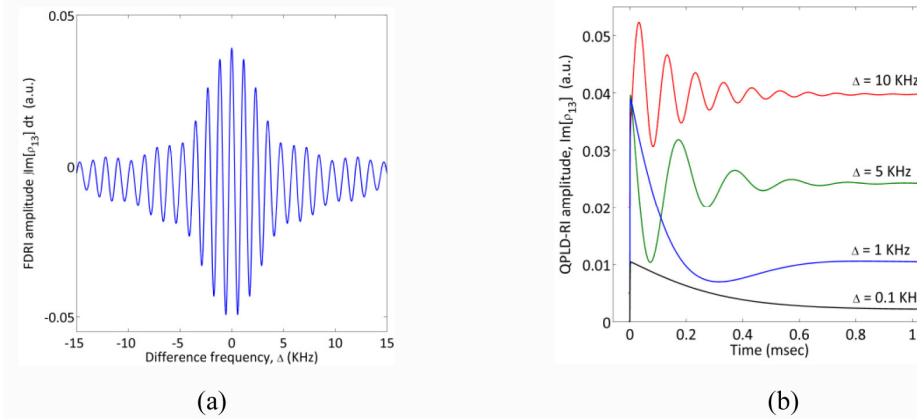


Fig. 4. Numerical solutions showing (a) FDRI obtained by using the pulse parameters as described in the text, (b) QPLD-RI corresponding to different values of Δ , as a function of the query pulse duration.

Figure 4b shows numerically computed QPLD-RI fringes for different values of Δ . In this case, an attenuated (average Rabi frequency $2\pi \cdot (\Gamma/50)$) query pulse was used, with τ_i and T chosen to be $212 \mu\text{s}$ and $508 \mu\text{s}$, respectively. Here, the horizontal axis is the duration of the query pulse, extending to a value exceeding 1 msec. Thus, these oscillations are in the time domain. The time period of these oscillations agree with $1/\Delta$, as expected. For a given value of Δ , the amplitude of the fringe now depends on the duration of the query pulse, in an oscillatory manner. Increasing the Rabi frequency (or Raman pumping rate α) of the query pulse causes a faster decay of the fringe amplitude. Negative values of Δ generate the same fringes as the positive values, but with a π phase shift. Thus, for a give value of large τ_2 , the fringe pattern as a function of Δ will be asymmetric, especially when $\beta \neq 0$. In addition, the width of the FDRI fringes will depend on the length of the query pulse. The asymmetry and the variation in the width can both serve as a potential source of error for atomic clocks, as discussed in greater detail later. Next, we present experimental results showing these interference effects generated in a buffer-gas filled rubidium vapor cell.

3. Experimental setup

Figure 5 shows the experimental setup used to study QPLD-RI and FDRI in ^{85}Rb atomic vapor. A 10 cm long vapor cell containing a natural mixture of Rb isotopes and Ne buffer gas at 10 torr pressure is used. An external-cavity diode laser (ECDL, Vortex Series, New Focus) operating at 795 nm is used for optical excitation of the D1 line transitions in ^{85}Rb atoms, and is locked to the ($F=3-F'=3$) transition using saturated absorption spectroscopy (SAS).

Part of the ECDL light is amplified by injection locking a slave laser with 1-2 mW seed power. This injection locked laser (ILL) uses a 150 mW diode that runs near 800 nm when not injection-locked. The ILL wavelength is monitored using an optical spectrum analyzer to ensure single-wavelength operation with >40 dB sidemode and pedestal suppression. This amplified light passes through an acousto-optic modulator (AOM) centered at 80 MHz that

can be switched on with $< 1 \mu\text{s}$ rise time. The frequency of this switched light, ω_1 , is also at the $F=3 - F'=3$ transition because it is compensated by an AOM in the SAS setup, which is not shown in the figure.

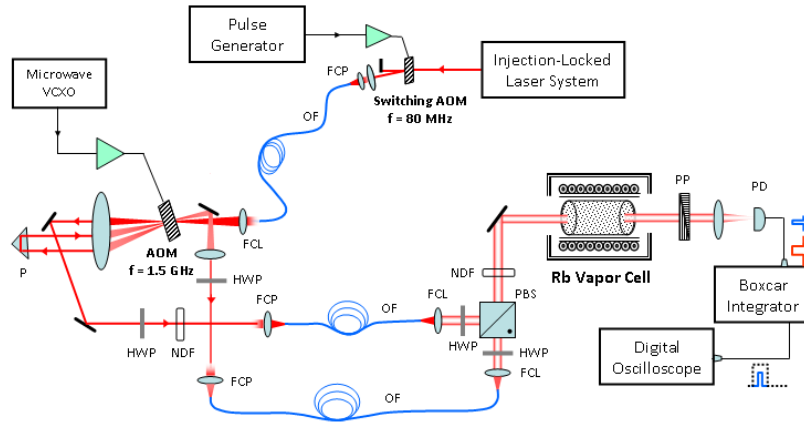


Fig. 5. Experimental setup for Ramsey interference consisting of an injection-locked diode laser, AOM for generating Raman beams and a buffer gas filled Rb cell. FCL: fiber collimating lens, FCP: fiber coupler, NDF: neutral density filter, OF: optical fiber, P: prism (out-of-plane as discussed in the text), PP: prism polarizer, PBS: polarizing beam splitter, PD: photodiode, and HWP: half-wave plate.

The frequency-shifted Raman beam at ω_2 is generated from ω_1 using a Bragg acousto optic modulator (AOM; $f = 1.5 \text{ GHz}$, $\text{BW} = \pm 100 \text{ MHz}$, Brimrose Corporation) in a double-pass configuration as shown in Fig. 5 for operation near the ground state hyperfine frequency ω_{hf} ($\approx 3.0357 \text{ GHz}$). A narrowband microwave voltage controlled oscillator (VCXO) driven near 1517.8 MHz allows us to vary the Raman detuning Δ over roughly 0.5 MHz (100 kHz/V). The input light for the AOM is fiber-delivered and focused to a spot size of 60 microns . Since the AOM diffraction efficiency is polarization dependent, use of a polarizing beam splitter at the input, in conjunction with a polarization rotation after the first pass, for separating the double-pass beam from the input, is not possible. Instead, The shifted beam after the first pass was spatially separated from the input beam by displacing the beam out-of-plane by a microprism and picked off by an edge mirror. The out-of-plane shift causes no noticeable reduction in diffraction efficiency, and the total double-pass efficiency of the AOM is $\sim 5\%$. The undeflected light (ω_1) and the deflected light (ω_2) are each coupled into separate polarization-maintaining (PM) fibers.

These two beams are collimated to $1/e^2$ diameters of 4 mm using fiber aspheres (Thorlabs C260TM-B, $f=15.36 \text{ mm}$) with near-Gaussian profiles and orthogonal, linear polarizations for Raman excitation. They are combined using a polarizing beam splitter for copropagating excitation. Both beams can be pulsed simultaneously using the AOM in the ILL setup, and Δ is changed by sweeping the VCXO.

The cell is magnetically shielded and heated to a steady-state temperature near 50° C for producing a moderate atomic density ($10^{12}/\text{cm}^3$). Helmholtz coils inside the shielding volume produced a small homogeneous axial field with flux density $\leq 100 \text{ mG}$. This causes an antisymmetric shift of the Zeeman sublevels and allows us to separate the Raman transitions between $|F=2, m_F=0\rangle$ and $|F=3, m_F=0\rangle$ (the so-called clock transition) from the other, magnetically-sensitive Raman transitions. The clock transition is insensitive to magnetic field to a first-order, but one can also choose magnetically-sensitive Raman transitions if interested in doing sensitive magnetometry.

A high extinction ratio Glan-Thompson polarizer (40 dB) is used after the vapor cell to remove one of the Raman beams from reaching the detector. Ramsey interference in the pulse amplitude is observed by a gated boxcar integrator [14] which generates an integrated signal corresponding to the amplitude of the query pulse. Note that Ramsey interference can also be observed without the prism polarizer since the effect is manifested in both Raman beams. The prism polarizer allows us to observe the effect at one frequency (ω_1 or ω_2) without being encumbered by the beating with the other.

4. Experimental results and discussions

Two different pulsed Raman excitation schemes are used in the experimental setup shown in Fig. 5 to generate QPLD-RI and FDRI in ^{85}Rb vapor. In both cases, relatively long CPT pulses ($\tau_1 = 200 \mu\text{s}$) are used for the initial Raman excitation. FDRI is observed by sending a repeated sequence of Raman pulse pairs (generated by the AOM in the ILL setup) consisting of a short query pulse ($\tau_2 = 400 \text{ ns}$), and by scanning the frequency of ω_2 to change the two-photon resonance condition. The pulse sequence is synchronized with the voltage ramp that controls the VCXO.

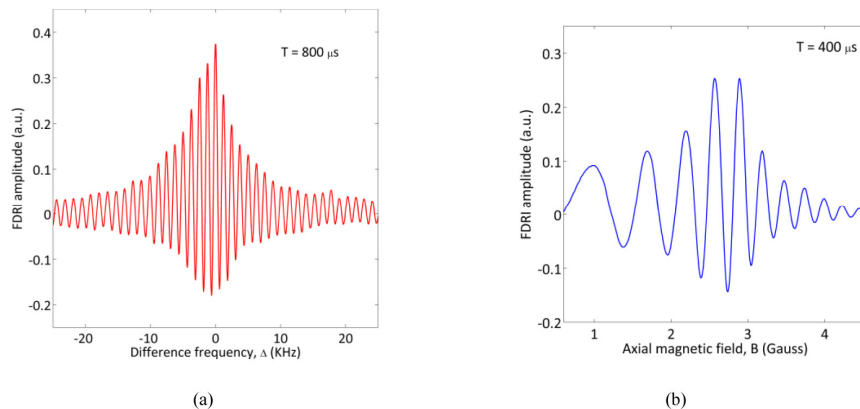


Fig. 6. (a) Experimentally observed FDRI using Raman excitation in the (0-0) ground-state 'clock transition' in ^{85}Rb vapor, (b) second-order magnetic field, B dependence of FDRI.

Figure 6a shows experimentally observed FDRI using $T = 800 \mu\text{s}$. The result qualitatively matches our numerical simulation shown earlier. The linewidth $\Delta\nu$ is inversely related to the free evolution time T between the Raman pulse pair and is measured to be close to 625 Hz. A total optical power of about $300 \mu\text{W}$ is used in the Raman beams and a power ratio of 2:1 between the Raman beams is used in this case, in order to ensure that the Rabi frequencies for the two legs of the Λ -transition are nearly equal, taking into account the different oscillator strengths along the two legs. In our experiments, T of up to 1.5 ms has been used to generate a fringe width as narrow as 330 Hz, with a signal-to-noise ratio of about 10. The maximum value of T is limited by the ground-state decoherence time in the medium.

The central frequency in the above experiment is defined by the $|F=2, m_F=0\rangle$ and $|F=3, m_F=0\rangle$ Raman transition in ^{85}Rb atoms. It has a quadratic (second-order) dependence on the magnetic field. The sensitivity of this frequency to the external magnetic field, B is verified by studying the magnetic field dependence of FDRI. This is done by changing the strength of axial magnetic field, B , linearly using the Helmholtz coil, and keeping the frequency difference between the Raman beams matched to the condition $\Delta = 0$ for $B=0$. Figure 6b shows FDRI fringes for $T = 400 \mu\text{s}$, while scanning B around a dc (or bias) magnetic field (approximately 2.5 G) so that it does not change its direction. The frequency of the interference pattern is chirped due to the quadratic dependence on B . This can be

described [23] as $I(B) \approx (1 - e^{-\eta\tau_2}) \cdot [1 + \cos(\alpha_{0-0} B^2 T)]$, where $\eta = \frac{\Gamma \xi}{1 + 3\xi}$, α_{0-0} ($= 1.293$ kHz/G²) is second-order magnetic field coefficient associated with the clock transition, while assuming that $\tau_1 \gg \tau_2$.

QPLD-RI was observed in the experiment by replacing the short detection pulse used in FDRI by a long, attenuated query pulse of duration up to $\tau_2 \approx 4$ ms in the Raman pulse sequence. In this case, Ramsey interference fringes were observed directly as time-domain oscillations in the amplitude of the query pulse without the use of boxcar integrator. The optical power in the query pulse was attenuated by nearly twenty times so that it does not cause any significant decay of coherence created by the first Raman pulse. Figure 7a shows QPLD-RI observed in the pulse amplitude due to Ramsey interference, as explained before. The vertical axis for each plot corresponding to different values of Δ is displaced in order to show all the plots together. The initial part of the plot also shows the first Raman pulse preceding the query pulse. For this experiment, τ_1 and T were chosen to be 400 μ s and 250 μ s, respectively. The period of these oscillations closely match with $1/\Delta$. The decay of the fringes is due to a combination of two effects: saturation of the system into the dark state, and decoherence due to collision. For our experiment, the decoherence is much faster than the rate at which the system decays to a dark state. Under this condition, the number of observed oscillations in QPLD-RI can be described as $I(\tau) \approx [1 + \cos(\Delta \cdot (\tau + T))] \exp(-\tau/t_c)$, where t_c is the ground-state decoherence time. Our results indicate that the coherence in the medium survives approximately for 3-4 ms. This illustrates the fact that the coherence survives many collisions as the atoms slowly diffuse in the interaction region in the presence of the buffer gas [25].

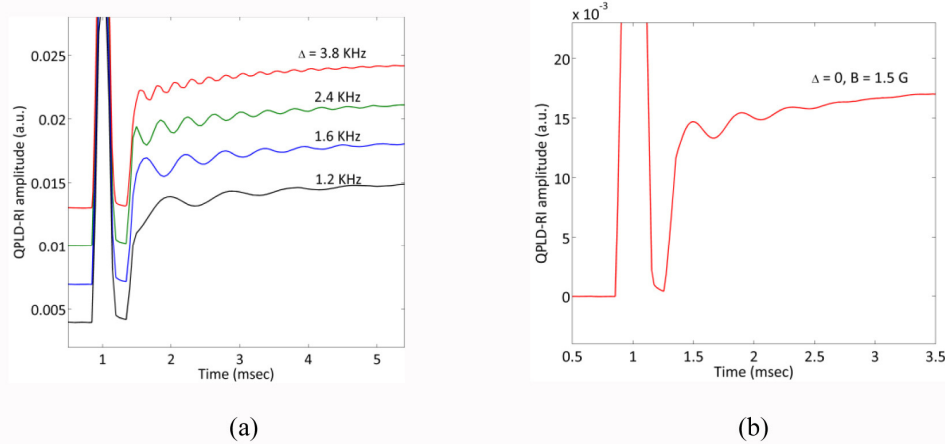


Fig. 7. (a) Experimentally observed QPLD-RI for different values of Δ as shown in the figure, (b) magnetic field dependence of QPLD-RI for $\Delta \approx 0$. The horizontal axis shows the whole pulse sequence.

Transient coherent oscillation has been reported by making changes to the Raman detuning for CPT fields [26]. We would like to point out that the effect reported in ref. 26 is quite different from QPLD-RI. The oscillations reported there was observed while changing the Raman detuning as a function of time, either abruptly or continuously. Furthermore, there was no dark time interval. In contrast, QPLD-RI is observed while the Raman detuning is kept constant, and there is a dark time interval between the initial excitation and the query pulse.

We have also studied the magnetic field dependence of QPLD-RI by applying different axial magnetic fields. Figure 7b shows QPLD-RI obtained by using $B = 1.5$ G, while keeping $\Delta \approx 0$. The pulse parameters chosen in this case are $\tau_1 = 400$ μs , $T = 250$ μs and $\tau_2 \approx 4$ ms. These oscillations can be described as $I(\tau) \approx \left[1 + \cos(\alpha_{0-0} B^2 (\tau + T))\right] \exp(-\tau/t_c)$. If a different magnetic field is applied, the periodicity of the fringes changes quadratically (not shown) with the field strength. The effective decoherence time measured from the decay of the fringe amplitude is shorter ($t_c \approx 2$ ms) compared to those shown in Fig. 7a. This is possibly due to the inhomogeneity of the axial magnetic field over the length of the cell.

Finally, we discuss how the QPLD-RI can affect the accuracy of an atomic clock under various conditions. Consider first the ideal case where the average optical detuning δ is set to zero. Figure 8 shows the effect of choosing different query pulse duration, τ_2 , on the FDRI fringes, using numerical calculations. The Rabi frequencies for Raman beams were chosen to be $\Omega_1 = \Omega_2 = 2\pi (I/5)$ during the first Raman pulse, and $\Omega_1 = \Omega_2 = 2\pi (I/200)$ during the second (or query) Raman. We used a repeated pulse sequence in the calculation, with pulse parameters $\tau_1 \approx 212$ μs and $T = 795$ μs , same as shown earlier. Here, we show only the central FDRI fringe (Fig. 8a), for three different query pulse durations: 10 μs , 100 μs , and 300 μs .

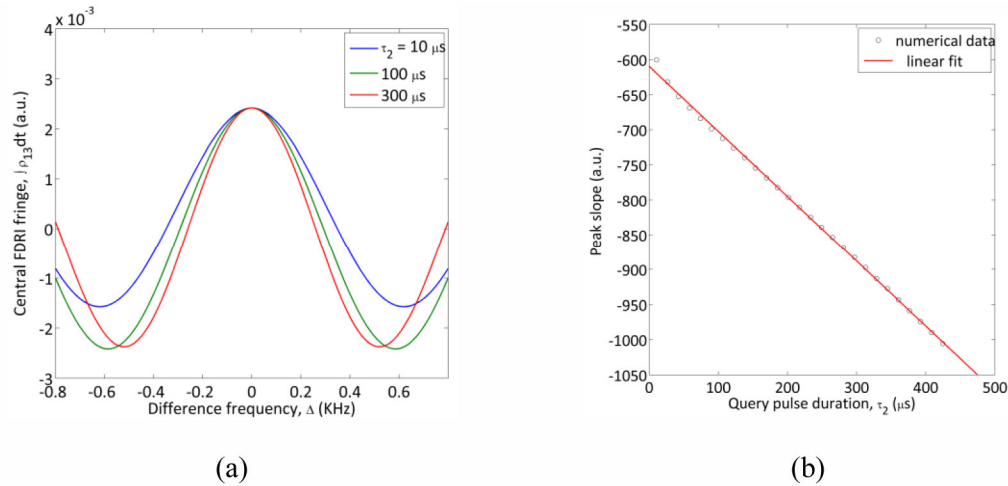


Fig. 8. Numerical results showing change in (a) central FDRI fringe width and (b) slope at the fringe center as a function of query pulse duration, τ_2 .

In Fig. 8b, we have plotted the central slope of the derivative of the fringes, for a range of query pulse durations, τ_2 . This slope is a measure of the width of each fringe. As can be seen, the slope increases with query pulse length, corresponding to narrowing of fringes. It is well known that the shot-noise limited fractional frequency stability (FFS) of a clock, stabilized to the center of one such fringe, is given by $(\gamma / f_0) / (S/N)$, where γ is the fringe width, f_0 is the central frequency of the clock (matching the frequency difference between $|3\rangle$ and $|1\rangle$), and (S/N) is the signal-to-noise ratio (SNR). Thus, for a given SNR, the FFS, which is the defining parameter for a clock used in any system, will vary if the query pulse length is varied. This dependence is currently not taken into account in considering the FFS of a pulsed Raman clock. A key message of this paper is that one must pay attention to the length of the query pulse in determining the FFS of such a clock.

Consider next the non-ideal case where the average detuning, δ , is non-zero. In any Raman clock, this condition is relevant in order to account for inevitable fluctuations in the laser frequency. For a vapor cell base Raman clock, this condition is also unavoidable because of the presence of several hyperfine transitions in the excited manifold that can all contribute

to the clock signal, due to Doppler broadening. For illustrative purposes, we first choose $\delta = -\Gamma$ in Fig. 9a. Here, we show the FDRI fringes for three different query pulse durations: 10 μs , 210 μs , and 300 μs . Note that in each case the center of the fringe peak is shifted from the ideal position of $\Delta = 0$. This shift is proportional to the intensity of the fields used in the first excitation pulse, and is thus a manifestation of the light-shift or the ac-Stark shift [23]. We see that as the query pulse length increases, the amount of shift changes, and the fringes become increasingly asymmetric. In Fig. 9b, we have plotted the shift as a function of the query pulse duration, for $\delta = -1.5\Gamma$. In this case, the variation is seen to be approximately linear; in general, the exact functional dependence of the shift on the query pulse is expected to be different for different choice of parameters. Currently, the laser linewidth, the Doppler width, the relative frequency separation between the hyperfine levels in the excited state manifold, and the dependence of light shift on δ together are used to estimate the light-shift induced limit of the clock accuracy for a vapor cell based Raman clock. From the result illustrated in Fig. 9, we conclude that the query pulse duration must also be taken into account in determining this limit accurately.

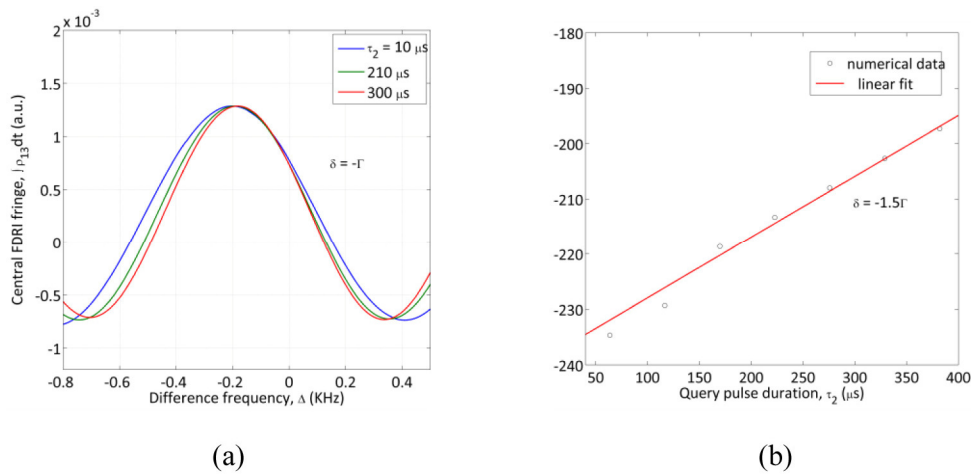


Fig. 9. Numerical results showing (a) light shift in central fringe for $\delta = -\Gamma$, and (b) variation in light shift as a function of τ_2 corresponding to $\delta = -1.5\Gamma$.

The results presented in this paper are only qualitative. For a quantitative determination of the effect of query pulse dependence for a vapor cell based Raman clock, one must take into account the Doppler shift for atoms moving in three dimensions, the hyperfine levels in the excited state manifold, the different strengths of the various transitions, and optical pumping into and out of various Zeeman sublevels. We are in the process of carrying out such an analysis. Until the comprehensive theoretical modeling is completed, we cannot expect to predict precisely the effects of QPLD-RI on the clock frequency fluctuations. Furthermore, in our clock setup, excess noise induced fluctuations are too large to observe these effects currently. Efforts are underway to improve our apparatus to reach shot-noise limited performance, so that these effects can be measured. We expect to report on the comprehensive theoretical model as well as experimental studies of these effects in the near future.

5. Conclusion

In summary, we have shown a new type of Ramsey interference effect, QPLD-RI, which is observed when a long, attenuated query pulse is used during pulsed Raman excitation in rubidium vapor. This effect can produce pulse length dependent broadening as well as asymmetry in FDRI fringes used for a vapor cell Raman clock, causing a potential source of error. Specifically, we have shown that broadening affects the fractional frequency stability of

a clock, and asymmetry changes the magnitude of the light-shift induced error due to optical detuning, which is unavoidable in a vapor cell based Raman clock because of the presence of several hyperfine transitions in the excited state manifold, which all contribute to the clock signal because of Doppler broadening. Thus, in choosing the optimal parameters for such a clock, the effect of QPLD-RI has to be taken into account. The origin of FDRI and QPLD-RI has been explained qualitatively using a Bloch vector model as well as numerical solutions to time-dependent density matrix equations.

Acknowledgments

This work was supported by NASA URC grant #NNX09AU90A, NSF-CREST grant #0630388 and AFOSR grant #FA9550-10-01-0228. The author G.S. Pati also acknowledges the financial support from the ONR Summer Faculty Program for giving him the opportunity to conduct this research at the Naval Research Laboratory (NRL), Washington, DC.